2018 European Control Conference (ECC)
June 12-15, 2018. Limassol, Cyprus

Entrainment in harmonically forced continuous and impulsive Goodwin's oscillators: a comparison study

Alexander Medvedev[1], Anton V. Proskurnikov[2,3,4], and Zhanybai T. Zhusubaliyev[5]

Abstract— **The Goodwin oscillator is a simple yet illustrative model of a biochemical system with a stable limit cycle. Considered as a prototypical biological oscillator, Goodwin's model is broadly used e.g. to describe circadian rhythms, hormonal cycles, self-oscillatory metabolic pathways. These periodic or non-periodic oscillations are self-sustained; at the same time, they are *entrainable* by external periodic signals, adjusting the characteristics of the autonomous oscillatory behavior. Mathematical analysis of entrainment phenomena, i.e. nonlinear phenomena imposed by periodic exogenous signals, remains an open problem. This paper presents a comparative analysis of forced dynamics arising in two versions of Goodwin's oscillator: the classical continuous oscillator and a more recent impulsive one, e.g. capturing pulsatile secretion of hormones. The main finding of this study is that while the continuous oscillator is always forced to a periodic solution by a sufficiently large exogenous signal amplitude, the impulsive one commonly exhibits a quasiperiodic or chaotic behavior thus highlighting the role of non-smooth dynamics in entrainment.**

I. Introduction

Many physiological variables in living organisms, from single-celled microbes [1] to mammals, exhibit a pronounced 24 hours cycle, called the *circadian rhythm*. Circadian rhythms are self-sustained and maintained by endogenous biological clocks, assembled of intracellular genetic oscillators. However, the circadian clock's frequency and phase can be adjusted by environmental "cues" (e.g. day-and-night change, temperature variations, physical activity and meals), referred in chronobiology to as *Zeitgebers* (time signals, synchronizers) [2]. This mechanism of *entrainment* plays an important role in the functioning of living organisms, adapting them to the changing environment.

In biology, entrainment of circadian rhythms has been studied for a long time, cf [3]. The research has been primarily focused on periodic solutions forced by exogenous periodic signals (e.g. the light-dark cycle), in particular, the influence of the external input on the endogenous oscillator's phase. The key characteristics of such an influence are phase response and phase transition curves [4], [5]. The highly nonlinear nature of entrainment gives rise to e.g. asymmetric phase response to time difference in long-haul air travel: eastward jet lag is worse than the westward kind [6].

*This work was supported by the Swedish Research Council, Grant 2015-05256 and RFBR grants 17-08-01728, 17-08-00715 and 17-08-01266.

[1]Department of Information Technology, Uppsala University, SE-751 05 Uppsala, Sweden alexander.medvedev@it.uu.se

[2]Delft Center for Systems and Control, Delft University of Technology, 2628 CD, Delft, The Netherlands; [3] ITMO University, 197101, St. Petersburg, Russia; [4] Institute for Problems of Mechanical Engineering, Russian Academy of Sciences (IPME RAS). anton.p.1982@ieee.org

[5] Department of Computer Science, Southwest State University, 50 Years of October Str., 94, 305040, Kursk, Russia zhanybai@hotmail.com

In this paper, entrainment is understood in a broader sense, namely, as a qualitative change in an oscillator's behavior due to a periodic exogenous force. The resulting forced solution is not always periodical; the periodic forcing of a circadian clock in fact may even lead to *chaotic* oscillations [7]. In this paper, entrainability properties of a simple model known as the Goodwin oscillator [8] are examined.

This paper presents a comparative study of the entrainment effects in continuous and impulsive Goodwin's models. The main contributions are as follows. The previously unknown occurrence of quasiperiodic solutions in a harmonically forced Goodwin's oscillator for small amplitudes of the exogenous signal is explained by bifurcation analysis. In agreement with analytical results, the model solutions become periodic for sufficiently large amplitude values. In the impulsive Goodwin's oscillator, large amplitudes of a periodic exogenous signal do not necessarily lead to periodicity of the solution but can result in either quasiperiodicity or chaos. Yet moderate magnitudes of the exogenous signal entrain quasiperiodic solutions and give rise to a periodic movement through a saddle-node bifurcation.

The rest of the paper is organized as follows. Section II introduces the classical continuous Goodwin's oscillator with a brief summary of its basic mathematical properties, followed up by a periodically forced version of the model in Section III. Section IV treats the forced impulsive Goodwin's oscillator through bifurcation analysis of its Poincaré map. The results are summed up in Conclusions.

II. Classical Goodwin's oscillator

The classical Goodwin's oscillator is given by

$$\begin{aligned} \dot{x}_1(t) &= -b_1 x_1(t) + h(x_3(t)) \\ \dot{x}_2(t) &= -b_2 x_2(t) + g_1 x_1(t) \\ \dot{x}_3(t) &= -b_3 x_3(t) + g_2 x_2(t). \end{aligned} \tag{1}$$

The state variables $x_i(t)$, $i = 1, 2, 3$, typically stand for the concentrations of some chemicals (e.g. the levels mRNA, protein and intermediate enzyme in the cell [8] or the blood levels of hormones [9]) and $b_i > 0$ are their constant clearing rates. The constants $g_1, g_2 > 0$ and a *non-increasing* nonlinearity $h(\cdot) \geq 0$ characterize the production rates of the chemicals; usually $\inf_{\xi \geq 0} h(\xi) = \lim_{\xi \to \infty} h(\xi) = 0$.

The nonlinearity $h(\cdot)$ closes the *negative feedback loop* and typically chosen to be the *Hill* function of order n [10]

$$h(\xi) = \frac{a}{1 + \mathcal{K}\,\xi^n}, \tag{2}$$

with $a > 0$, $\mathcal{K} > 0$ (the exponent $n > 0$ is usually integer).

Intuitively, this system functions as follows. When the level of Chemical 3 is low, the production rate of Chemical 1 is near its maximum, thus accelerating production of Chemical 2 (since $g_1 > 0$) and, indirectly, Chemical 3 (since $g_2 > 0$). On the other hand, a high concentration of Chemical 3 corresponds to a low production rate of Chemical 1, which also decelerates the production of Chemical 2 and Chemical 3. Goodwin reported that such a feedback mechanisms may exhibit a stable limit cycle. The necessity of a limit cycle in the oscillator has motivated Goodwin (and earlier Danziger and Elmergreen) to consider a chain of three reactions. Systems of two coupled reactions usually can exhibit self-sustained oscillations only when they have a nested family of closed orbits (like in the usual harmonic oscillator, the equilibrium is the *center*) [11], [8]. Earlier, it has been noticed [12] that (1),(2) with $n \leq 8$ always has a stable equilibrium, whereas for $n > 8$ the system can have stable periodic orbits, arising through the Hopf bifurcation. Main local and global properties of the Goodwin oscillator are now formulated.

A. Stability, cycles and bifurcations in the Goodwin's model

Introducing $\mathbf{x}(t) = [x_1, x_2, x_3]^T$, (1) is rewritten as

$$\begin{aligned} \frac{d\mathbf{x}}{dt} &= \mathbf{f}(\mathbf{x}) = \mathbf{A}\mathbf{x} + \mathbf{B}h(x_3), \\ \mathbf{A} &= \begin{bmatrix} -b_1 & 0 & 0 \\ g_1 & -b_2 & 0 \\ 0 & g_2 & -b_3 \end{bmatrix}, \quad \mathbf{B} = \begin{bmatrix} 1 \\ 0 \\ 0 \end{bmatrix}. \end{aligned} \tag{3}$$

Since $\mathbf{A}$ is Hurwitz and Metzler, whereas the vector $\mathbf{B}$ is non-negative and $h(x_3) \geq 0$ for $x_3 \geq 0$, the linear dynamics are stable and positive: any solution starting at $\mathbf{x}(0) \geq 0$ remains non-negative $\mathbf{x}(t) \geq 0$. Since $h(x_3)$ is bounded $0 \leq h(x_3) \leq h(0)$, all such solutions are bounded and exist up to ∞. The point $\mathbf{x}_*$ is an equilibrium of (1) if and only if

$$\begin{aligned} &-b_1 x_1^* + h(x_3^*) = g_1 x_1^* - b_2 x_2^* = g_2 x_2^* - b_3 x_3^* = 0 \\ &\Leftrightarrow \begin{cases} x_1^* = \dfrac{b_2}{g_1} x_2^* = \dfrac{b_2 b_3}{g_1 g_2} x_3^*, \quad x_2^* = \dfrac{b_3}{g_2} x_3^*, \\ x_3^* = c\, h(x_3^*), \quad c = \dfrac{g_1 g_2}{b_1 b_2 b_3} > 0. \end{cases} \end{aligned} \tag{4}$$

Since the function $h(\cdot)$ is non-increasing, the latter equation has the only (non-negative) root $x_3^* \geq 0$, corresponding to the unique biologically feasible equilibrium $\mathbf{x}_* \geq 0$.

Henceforth, h is assumed to be continuously differentiable in the vicinity of x_3^*; note that $h'(x_3^*) \leq 0$ since h is non-increasing. Stability properties of the unique equilibrium are determined by the eigenvalues of the Jacobian matrix

$$\mathbf{Df}(\mathbf{x}_*) = \begin{bmatrix} -b_1 & 0 & h'(x_3^*) \\ g_1 & -b_2 & 0 \\ 0 & g_2 & -b_3 \end{bmatrix}, \tag{5}$$

that is, the zeros of its characteristic polynomial

$$\begin{aligned} &\det\left(\lambda \mathbf{I} - \mathbf{Df}(\mathbf{x}_*)\right) = \lambda^3 + a_1\lambda^2 + a_2\lambda + a_3 = 0, \\ &a_1 = b_1 + b_2 + b_3 > 0, \\ &a_2 = b_1\, b_2 + b_1\, b_3 + b_2\, b_3 > 0, \\ &a_3 = b_1\, b_2\, b_3 - g_1 g_2 h'(x_3^*) \geq b_1\, b_2\, b_3 > 0. \end{aligned} \tag{6}$$

Using the Routh-Hurwitz criterion, the equilibrium of (1) is stable if $\Theta = a_1 a_2 - a_3 < 0$ and unstable when $\Theta > 0$. This leads to the following lemma improving over the original formulation in [9].

Lemma 1: [13] If $\mathcal{M}(\xi) = (-\xi h'(\xi)/h(\xi)) < 8$ for any $\xi \geq 0$, then the equilibrium is stable for all $b_i, g_i > 0$. If $\sup_{\xi \geq 0} \mathcal{M}(\xi) > 8$, the discriminant $\Theta = a_1 a_2 - a_3$ can be both positive and negative, depending on $b_i, g_i > 0$, and the system undergoes an Andronov-Hopf bifurcation as $\Theta = 0$.

Corollary 1: For Goodwin's oscillator in (1) with Hill nonlinearity (2), the equilibrium is locally stable whenever $n \leq 8$. When $n > 8$, the system may have unstable equlibrium and undergoes the Hopf bifurcation as $\Theta = 0$.

The global stability of the equilibrium when $\mathcal{M}(\xi) < 8$ remains a non-trivial problem. Some sufficient conditions are given by the "global" version of the secant criterion [14] and monotonicity-based criteria [15], [16], [17], which imply, in particular, that the equilibrium of (1),(2) with $n = 1$ is always globally attractive. Simulations show that the same holds for any $n \leq 8$, but the proof is still elusive.

A fundamental property of Goodwin's oscillator is the existence of a non-trivial periodic orbit in the case when the (unique) equilibrium is unstable.

Theorem 1: [18] Let $h \in C^1$ and the equilibrium $\mathbf{x}_*$ be unstable, i.e. some eigenvalue of $\mathbf{Df}(\mathbf{x}_*)$ has a positive real part. Then system (1),(2) has a (non-constant) periodic orbit. Furthermore, almost all trajectories converge to such orbits.

For $h \in C^2$, the first statement of Theorem 1 has been proved in [19]. The uniqueness of a periodic orbit in the Goodwin model remains an open problem. In presence of delays, such an orbit is in general non-unique [20].

B. Bifurcation analysis

Fig. 1a depicts the Andronov-Hopf bifurcation for $n = 9$ producing the oscillatory dynamics. For $b_1 < b_1^L$, the system possesses a stable equilibrium $\mathbf{x}_*$. For this parameter interval, Jacobian (5) has a pair of complex-conjugated eigenvalues $\lambda_{1,2} = \mu \pm i\omega$ with negative real parts $\mu < 0$, and one negative real eigenvalue $\lambda_3 < 0$. At the point $b_1 = b_1^L$, the equilibrium state undergoes an Andronov-Hopf bifurcation. When the parameter b_1 passes through the value $b_1 = b_1^L$ (Fig. 1b), a pair of complex-conjugated eigenvalues $\lambda_{1,2} = \mu \pm i\omega$ crosses the imaginary axis into the positive real half-plane. As a result, the equilibrium state becomes unstable, and a stable limit cycle appears. With further increase in the value of b_1, the unstable equilibrium point undergoes a reverse Andronov-Hopf bifurcation at the point $b_1 = b_1^R$, in which a stable limit cycle turns into a stable equilibrium state (Figs. 1a,b). In the bifurcation diagram Fig. 1a, the oscillatory state exhibits maximum and minimum values in the temporal variation of the state variable x_3. The maximum and minimum values of the state variable x_3 correspond to the points where phase trajectories intersect the surface $S = \{\mathbf{x} : g_2 x_2 - b_3 x_3 = 0\}$ in the phase space of system (1),(2) from the two directions (two-sided Poincaré map).

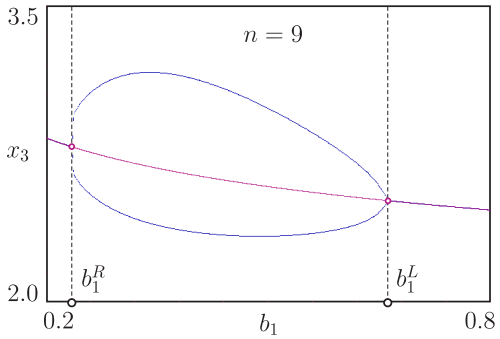

(a)

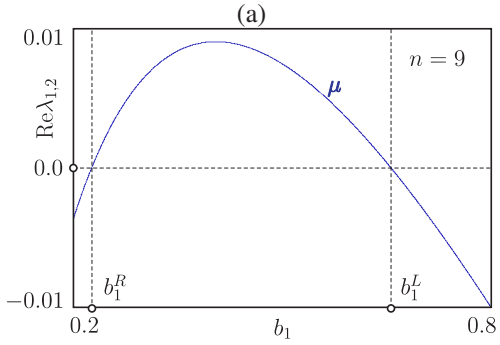

(b)

Fig. 1: Birth of a limit cycle from a stable equilibrium point in an Andronov-Hopf bifurcation. $n = 9$, $b_2 = 0.5$, $b_3 = 0.3$, $g_1 = 2.0$, $g_2 = 0.5$, $a = 100$, $\mathcal{K} = 0.1$ and $0.2 < b_1 < 0.8$. (a) Bifurcation diagram. b_1^L and b_1^R are the Andronov-Hopf bifurcation points. (b) Variation of the real part $\mathrm{Re}\lambda_{1,2} = \mu$ of eigenvalues $\lambda_{1,2} = \mu \pm i\omega$. Note that $\lambda_3 < 0$.

III. Forced continuous Goodwin's model

Consider a Goodwin's oscillator subject to a positive single-tone harmonic exogenous signal $\beta(t) = M(1 + \sin(\omega t + \theta))$ of the period $T_\beta = 2\pi/\omega$

$$\begin{aligned} \dot{x}_1(t) &= -b_1 x_1(t) + h(x_3(t)), \\ \dot{x}_2(t) &= -b_2 x_2(t) + g_1 x_1(t), \\ \dot{x}_3(t) &= -b_3 x_3(t) + g_2 x_2(t) + \beta(t), \end{aligned} \tag{7}$$

that can be rewritten in the matrix form as follows

$$\frac{d\mathbf{x}}{dt} = \mathbf{f}(t, \mathbf{x}) = \mathbf{A}\mathbf{x} + \mathbf{B}h(x_3) + \mathbf{B_0}\beta(t),$$

where $\mathbf{A}, \mathbf{B}$ are defined in (3) and $\mathbf{B_0} = [0, 0, 1]^T$.

A. General entrainment properties

The general result of [21], dealing with forced oscillations in Lur'e-type systems with bounded slope-restricted nonlinearities, implies the following properties of (7).

Theorem 2: Let h and h' be bounded and $h'(\xi) \to 0$ as $\xi \to \infty$. For any $M > 0$, system (7) has a T_β-periodic solution (evidently, non-constant) $\mathbf{x}_M(t) = \mathbf{x}_M(t + T_\beta)$. For large $M > 0$, such a solution is unique and *locally* stable.

Theorem 2 follows from Theorem 1 and Theorem 2 in [21]. The proof of the latter allows to estimate the amplitude M_0 such that the uniqueness is guaranteed for any $M > M_0$, but the estimate appears to be conservative. For large M, the solution $\mathbf{x}_M(t)$ is close (uniformly in t) to the function $M\mathbf{x}_+(t)$ [21] , where $\mathbf{x}_+(t)$ is the unique T_β-periodic solution of the exponentially stable linear system

$$\frac{d\mathbf{x}_+}{dt} = \mathbf{A}\mathbf{x}_+ + \mathbf{B_0}\beta(t), \quad \mathbf{x}_+(t) = \mathbf{x}_+(t + T_\beta).$$

Theorem 2 remains valid for non-harmonic periodic signal $\beta(t)$ (under conditions of non-degeneracy [21]) and many nonlinear systems, different from Goodwin's oscillator (1) (e.g. "repressilators" and "promotilators" [22]). The forced system has a periodic solution even when the equilibrium of autonomous system (1) (i.e. for $M = 0$) is stable (e.g. h is the Hill function (2) with $n \leq 8$); the solution $x_M(t)$ is then also stable when $M \approx 0$. If the equilibrium of (1) is unstable, then the periodic solution of (7) is usually also unstable when M is small (unless T_β coincides with the period of self-oscillation, $\mathbf{x}_M(t)$ is close to the equilibrium $\mathbf{x}_*$ when $M \approx 0$). In the next subsection, the dynamics of forced Goodwin oscillator (7) are studied numerically.

B. Bifurcation analysis

Consider system (7) with Hill nonlinearity (2), where $n = 9$, $a = 100$, $\mathcal{K} = 0.1$ and other parameters as as follows $b_1 = 0.4$, $b_2 = 0.5$, $b_3 = 0.3$, $g_1 = 2.0$, $g_2 = 0.5$, $0 < M < 0.055$, $\omega = 2\pi/T_\beta$, $T_\beta = 2\pi/\omega = 1440$, $\theta = 0.0$.

A period-T_β solution $\mathbf{x}_M(t)$ of (7) corresponds to the fixed point of the stroboscopic map $\mathbf{x}(t) \mapsto \mathbf{x}(t + T_\beta)$. The fixed point of this map is located using the Newton-Raphson algorithm that allows not only to evaluate stable cycles but also unstable ones. To test stability of the periodic solutions, one computes the eigenvalues ρ_1, ρ_2, ρ_3 (henceforth $|\rho_1| \geq |\rho_2| \geq |\rho_3|$) of the monodromy matrix $\Phi(T_\beta)$ that satisfies

$$\frac{d\Phi(t)}{dt} = \mathbf{Df}(t, \mathbf{x}_M)\Phi(t), \quad \Phi(0) = I.$$

Fig. 2a shows a one-dimensional bifurcation diagram calculated for $0 < M < 0.055$ and constructed from a Poincaré section in the phase space of (7). For large amplitudes M of the forcing signal $\beta(t)$, (7) exhibits a stable period-T_β solution. As M is reduced, this solution undergoes an Andronov-Hopf bifurcation (or a Neimark-Sacker bifurcation for the fixed point in the corresponding Poincaré map), and loses stability when the absolute value of the complex-conjugate multipliers $|\rho_1| = |\rho_2|$ becomes greater than one.

The variation of $\rho_{1,2}$ is shown in Fig. 2b. The pair of complex-conjugate multipliers leaves the unit circle at a point $M = M_\varphi$. The stability loss of the cycle leads to the soft appearance of two-frequency quasiperiodic oscillations corresponding to a two-dimensional invariant torus T_q in the phase space of (7), and the intersection of T_q with the Poincaré section corresponds to the closed invariant curve C_a of the Poincaré map. Fig. 2c presents the phase portrait of (7) after the Andronov-Hopf bifurcation for $M = 0.035$.

As emphasized in Sec. II, autonomous system (1),(2) has no periodic orbits for $n \leqslant 8$. Simulation shows that the

forced continuous Goodwin's oscillator in (7) exhibits only a period-T_β solution for $n \leqslant 8$ (see Fig. 2d).

IV. Forced impulsive Goodwin's oscillator

In the impulsive Goodwin's oscillator [23], the feedback nonlinearity $h(\cdot)$ in (7) is substituted with a pulse-modulation mechanism thus introducing hybrid dynamics. The state of the forced continuous part is given by

$$\frac{d\mathbf{x}}{dt} = \mathbf{A}\mathbf{x} + \mathbf{B_0}\beta(t), \tag{8}$$

where $x_1(t)$ undergoes jumps at the time instants t_k, $k \geqslant 0$

$$x_1(t_k^+) = x_1(t_k^-) + \lambda_k, \quad t_{k+1} = t_k + T_k,$$

whose timing and magnitudes are specified by the amplitude and frequency modulation functions

$$\lambda_k = F(x_3(t_k)), \quad T_k = \Phi(x_3(t_k)).$$

The superscripts " $-$ " and " $+$ " denote the left- and right-side limits, respectively. A distinctive property of the impulsive Goodwin's oscillator is lack of equilibria [23] that resolves the issues with asymptotically stable equilibria in the continuous version of the model outlined Corollary 1.

Note that any solution $\mathbf{x}(t)$ to (8) can be written as $\mathbf{x}(t) = \mathbf{x}_p(t) + \mathbf{B_0}\vartheta(t)$, where $\mathbf{x}_p(t)$ is governed by

$$\frac{d\mathbf{x}_p}{dt} = \mathbf{A}\mathbf{x}_p(t), \quad \mathbf{x}_p(t_k^+) = \mathbf{x}_p(t_k^-) + \lambda_n\mathbf{B},$$

and $\vartheta(t)$ satisfies $\dot\vartheta(t) = -b_3\vartheta(t) + \beta(t)$. For simplicity of the index notation, rename the components of the continuous state vector $\mathbf{x}_p^T(t) = [x(t) \quad y(t) \quad z(t)]$.

In continuously forced model (8), the impulse times t_k and the weights λ_k are modified by $\vartheta(t)$. Since $x_3(t) = z(t) + \vartheta(t)$, then

$$t_{k+1} = t_k + \Phi(z(t_k^-) + \vartheta(t_k)),\ \lambda_k = F(z(t_k^-) + \vartheta(t_k)).$$

Here $\vartheta(t)) = \frac{M}{b_3^2+\omega^2}\left[b_3\sin(\omega t + \theta) - \omega\cos(\omega t + \theta)\right] + \frac{M}{b_3}$.

Introduce $\varphi = \omega t$ and $x(t_k^-) = x_k$, $y(t_k^-) = y_k$, $z(t_k^-) = z_k$, $\varphi(t_k) = \varphi_k$. In this way $\varphi_{k+1} = \varphi_k + \Phi(z_k + \vartheta(\varphi_k))$ and $\lambda_k = F(z_k + \vartheta(\varphi_k))$. Then the Poincaré map of the forced model in (8) can be rewritten as [24]

$$\begin{aligned}
x_{k+1} &= \mathrm{e}^{-b_1T_k}(x_k + \lambda_k), \\
y_{k+1} &= E_{21}(T_k)(x_k + \lambda_k) + \mathrm{e}^{-b_2T_k}y_k, \\
z_{k+1} &= E_{31}(T_k)(x_k + \lambda_k) + E_{32}(T_k)y_k + \mathrm{e}^{-b_3T_k}z_k, \\
\varphi_{k+1} &= \varphi_k + \omega\,T_k \pmod{2\pi}, \quad k = 0, 1, 2, ...,
\end{aligned} \tag{9}$$

with

$$\begin{gathered}
T_k = \Phi(\sigma_k), \quad \lambda_k = F(\sigma_k), \\
\sigma_k = z_k + \frac{M}{b_3^2+\omega^2}\left[b_3\sin(\varphi_k + \theta) - \omega\cos(\varphi_k + \theta)\right] + \frac{M}{b_3}, \\
0 \leqslant \varphi_k \leqslant 2\pi, \quad 0 \leqslant \theta \leqslant 2\pi.
\end{gathered}$$

Here

$$\begin{gathered}
E_{21}(T) = \frac{g_1}{b_2 - b_1}(\mathrm{e}^{-b_1T} - \mathrm{e}^{-b_2T}), \\
E_{32}(T) = \frac{g_2}{b_3 - b_2}(\mathrm{e}^{-b_2T} - \mathrm{e}^{-b_3T}), \\
E_{31}(T) = \alpha_1\mathrm{e}^{-b_1T} + \alpha_2\mathrm{e}^{-b_2T} + \alpha_3\mathrm{e}^{-b_3T}, \\
\alpha_1 = \frac{g_1g_2}{(b_2 - b_1)(b_3 - b_1)}, \ \alpha_2 = \frac{g_1g_2}{(b_1 - b_2)(b_3 - b_2)}, \\
\alpha_3 = \frac{g_1g_2}{(b_1 - b_3)(b_2 - b_3)}.
\end{gathered}$$

The modulation functions of the intrinsic pulsatile feedback are selected as

$$\Phi(\sigma) = k_1 + k_2\frac{(\sigma/r)^n}{1 + (\sigma/r)^n}, \quad F(\sigma) = k_3 + \frac{k_4}{1 + (\sigma/r)^n}.$$

The introduction of the exogenous signal β modifies the argument of the modulation function and can be effectively interpreted as time-dependence of $F(\cdot)$ and $\Phi(\cdot)$. Yet, compared to the autonomous case, bistability appears in the forced system dynamics, [24]. Another crucial observation is that $\sigma_k \geq x_k$ due to the positivity of the exogenous signal. Since the modulation functions $F(\cdot)$ and $\Phi(\cdot)$ are bounded from below and above, the modulation depth is reduced by $\beta \geq 0$ thus resulting in a smaller range of λ_k, T_k.

In contrast with the continuous Goodwin's oscillator, the impulsive version of the model is shown to agree well with biological data [25], [26].

A. Bifurcation analysis

The parameter values are selected as: $0.0 \leqslant M \leqslant 12.0$, $0.23 < b_1 < 0.69$, $b_2 = 0.014$, $b_3 = 0.15$, $g_1 = 0.6$, $g_2 = 1.5$, $k_1 = 50$, $k_2 = 220.0$, $k_3 = 1.5$, $k_4 = 5.0$, $r = 2.7$, $n = 3$. In the following analysis, the amplitudes of the forcing signal M and b_1 are used as the bifurcation parameters.

For a relatively small amplitude M, map (9) displays a quasiperiodic orbit. As M increases, the system enters the 1:7 entrainment region (or phase-locked region) via a saddle-node bifurcation at the point $M_{\mathcal{L}}$. This transition is shown in Fig. 3a for $b_1 = 0.5$. On the part of the bifurcation diagram in Fig. 3a that falls to the left of the point $M_{\mathcal{L}}$, map (9) has a stable closed invariant curve, associated with quasiperiodic dynamics, as illustrated in Fig. 3b. The saddle-node bifurcation at the edge of the entrainment region produces a new attracting closed invariant curve (Fig. 3c). This closed curve includes two 14-cycles, a saddle and stable node, and is formed by the saddle-node connection composed of the unstable manifolds $W_{\pm}^U$ of the saddle cycle. In this way, inside the entrainment region, map (9) has the stable and saddle 14-cycles. The green lines in Fig. 3a (marked with 1) represent the saddle 14-cycle and the magenta lines (marked with 2) represent the stable 14-cycle.

With further increase of the forcing signal amplitude M, the invariant curve loses its smoothness at the point of the stable node 14-cycle due to folding of the unstable manifold W_+^U of the saddle 14-cycle and transforms to a folded set (Fig. 3d). This leads to the destruction of the closed curve [27]. Finally, the saddle and stable node 14-cycles

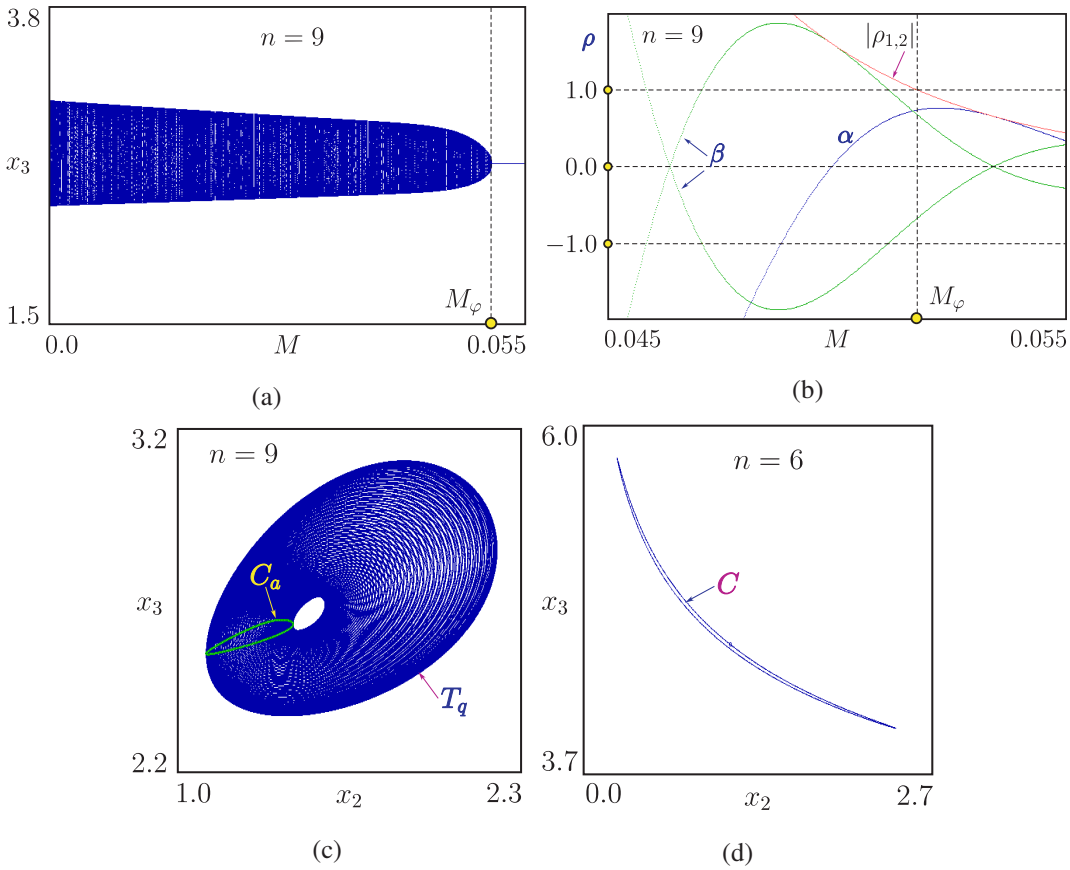

Fig. 2: Periodic and quasi-periodic solutions in continuously forced Goodwin's oscillator: (a) Bifurcation diagram illustrating the appearance of the two-dimensional torus through a Andronov-Hopf bifurcation. $b_1 = 0.4$, $b_2 = 0.5$, $b_3 = 0.3$, $g_1 = 2.0$, $g_2 = 0.5$, $a = 100$, $\mathcal{K} = 0.1$, $n = 9$, $0.0 < M < 0.055$. M_φ is the bifurcation point. (b) Multiplier diagrams for the stable 1-cycle, $0.045 < M < 0.055$. As the parameter M decreases, a pair of complex-conjugated multipliers $\rho_{1,2} = \alpha \pm i\beta$ of the 1-cycle leave the unit circle at the point $M = M_\varphi$. (c) Two-dimensional projection of the phase portrait after the Andronov-Hopf bifurcation for $M = 0.035$. Here T_q is the two-dimensional torus associated with the quasiperiodic solution of (7) and C_a denotes a closed invariant curve C_a of the corresponding Poincaré map. (d) Two-dimensional projection onto the plan (x_2, x_3) of the period-T_β solution for $n = 6$ and $M = 0.6$.

merge and disappear through a saddle-node bifurcation at $M_\mathcal{R}$ as the system leaves the entrainment region. This bifurcation creates a chaotic attractor (Fig. 3e).

Conclusions

The dynamics of two harmonically forced models of Goodwin's oscillator are studied by means of bifurcation analysis with emphasis on entrainment phenomena. In the classical continuous model, quasiperiodic solutions are discovered for small amplitudes of the exogenous signal that, in an Andronov-Hopf bifurcation, become periodic with an amplitude increase. Hybrid dynamics lead to much more complex scenarios in the case of the impulsive Goodwin's oscillator, where periodic solutions are observed for moderate values of the exogenous signal, while small and high amplitudes of it can result in quasiperiodicity or deterministic chaos. Another characteristic phenomenon appearing in the forced impulsive Goodwin's oscillator is the transitions from phase-locked dynamics to quasiperiodicity and chaos that are controlled by the phase of the exogenous signal.

References

[1] K. Whitehead, M. Pan, K. Masumura, R. Bonneau, and N. S. Baliga, "Diurnally entrained anticipatory behavior in Archaea," *PLoS ONE*, vol. 4, no. 5, p. e5485, 2009.

[2] J. Aschoff, M. Fatranská, H. Giedke, P. Doerr, D. Stamm, and H. Wisser, "Human circadian rhythms in continuous darkness: Entrainment by social cues," *Science*, vol. 171, no. 3967, pp. 213–215, 1971.

[3] J. de Mairan, "Observation botanique," *Hist. Acad. Roy. Sci.*, pp. 35–36, 1729.

[4] T. Roenneberg, S. Daan, and M. Merrow, "The art of entrainment," *J. of Biol. Rhythms*, vol. 18, no. 3, pp. 183–194, 2003.

[5] P. Sacre and R. Sepulchre, "Sensitivity analysis of oscillator models in the space of phase-response curves: Oscillators as open systems," *IEEE Control Syst. Mag.*, vol. 34, no. 2, pp. 50–74, 2014.

[6] Z. Lu, K. Klein-Cardena, S. Lee, T. M. Antonsen, M. Girvan, and E. Ott, "Resynchronization of circadian oscillators and the east-west asymmetry of jet-lag," *Chaos*, vol. 26, no. 9, 2016.

[7] D. Gonze and A. Goldbeter, "Entrainment versus chaos in a model for a circadian oscillator driven by light-dark cycles," *J. of Stat. Phys.*, vol. 101, no. 1-2, pp. 649–663, 2000.

[8] B. C. Goodwin, "Oscillatory behavior in enzymatic control processes," in *Advances of Enzime Regulation*, G. Weber, Ed., vol. 3. Oxford: Pergamon, 1965, pp. 425–438.

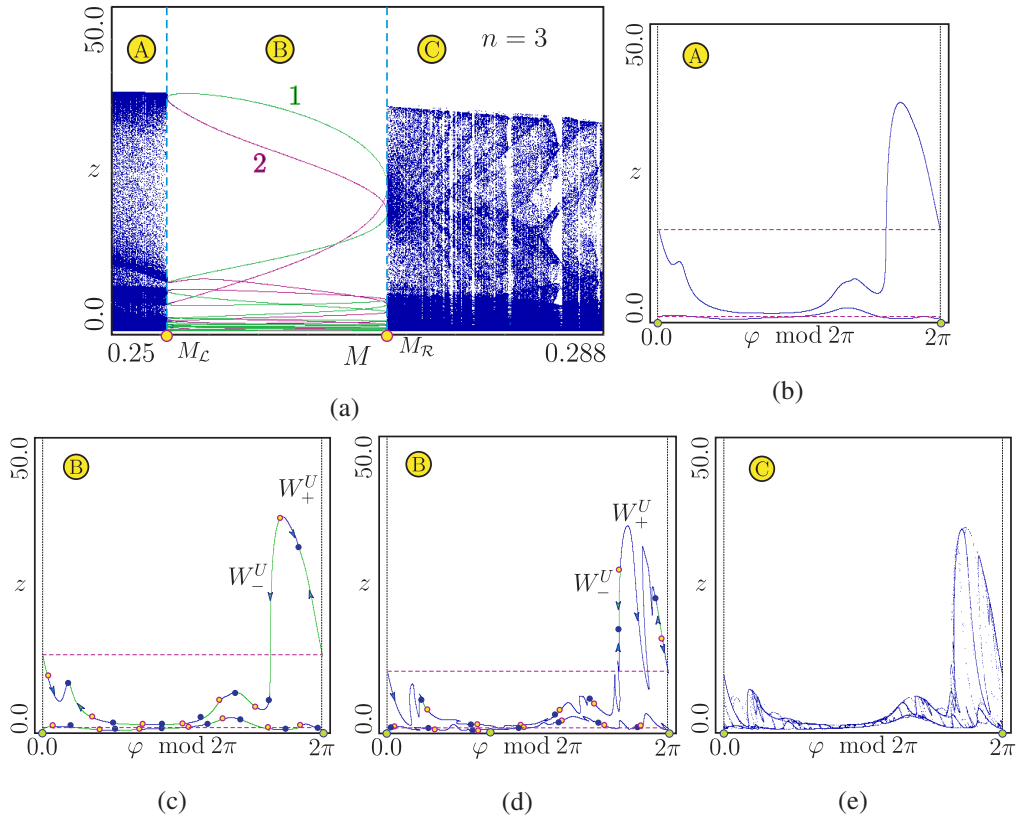

Fig. 3: (a) Bifurcation diagram showing the transition from a quasiperiodic orbit to a period-14 resonant dynamics in a saddle-node bifurcation with subsequent transition to a chaotic attractor through loss of smoothness and destruction of the invariant curve. $0.25 \leqslant M \leqslant 0.288$. $b_1 = 0.5$, $n = 3$. (b) Phase portrait of the map before the saddle-node bifurcation at $M_{\mathcal{L}}$. $M = 0.252$. (c) Phase portrait of the map after the saddle-node bifurcation. $M = 0.258$. Here, solid circles mark the stable 14-cycle and open circles mark the saddle ones. $W^U_{\pm}$ are unstable manifolds of the saddle 14-cycle. (d) Phase portrait of the map near the second saddle-node bifurcation at $M_{\mathcal{R}}$, $M = 0.27$. (e) Phase portrait of the map when the system lives the entrainment region (after the destruction of the closed invariant curve). $M = 0.2732$.

[9] W. R. Smith, "Hypothalamic regulation of pituitary secretion of lutheinizing hormone—II Feedback control of gonadotropin secretion," *Bull. Math. Biol.*, vol. 42, pp. 57–78, 1980.

[10] D. Gonze and W. Abou-Jaoude, "The Goodwin model: Behind the Hill function," *PLoS One*, vol. 8, no. 8, p. e69573, 2013.

[11] L. Danziger and G. Elmergreen, "The thyroid-pituitary homeostatic mechanism," *Bull. Math. Biophys.*, vol. 18, pp. 1–13, 1956.

[12] J. S. Griffith, "Mathematics of cellular control processes. i. negative feedback to one gene." *Journal of Theoretical Biology*, vol. 20, pp. 202–208, 1968.

[13] H. Taghvafard, A. Proskurnikov, and M. Cao, "Stability properties of the Goodwin-Smith oscillator model with additional feedback," *IFAC-PapersOnLine*, vol. 49, no. 14, pp. 131–136, 2016.

[14] M. Arcak and E. Sontag, "Diagonal stability of a class of cyclic systems and its connection with the secant criterion," *Automatica*, vol. 42, pp. 1531–1537, 2006.

[15] D. J. Allwright, "A global stability criterion for simple control loops," *Journal of Mathematical Biology*, vol. 4, pp. 363–373, 1977.

[16] G. Enciso and E. Sontag, "On the stability of a model of testosterone dynamics," *J. Math. Biol.*, vol. 49, no. 6, pp. 627–634, 2004.

[17] G. Enciso, H. Smith, and E. Sontag, "Nonmonotone systems decomposable into monotone systems with negative feedback," *J. Differential Equations*, vol. 224, p. 205 227, 2006.

[18] H. Taghvafard, A. V. Proskurnikov, and M. Cao, "Local and global analysis of endocrine regulation as a non-cyclic feedback system," *Automatica*, vol. 91, pp. 190–196, 2018.

[19] S. Hastings, J. Tyson, and D. Webster, "Existence of periodic solutions for negative feedback cellular control systems," *J. Differential Equations*, vol. 25, pp. 39–64, 1977.

[20] X. Sun, R. Yuan, and J. Cao, "Bifurcations for Goodwin model with three delays," *Nonlin. Dynamics*, vol. 84, pp. 1093–1105, 2016.

[21] A. Proskurnikov, M. Cao, and H.-T. Zhang, "Entrainment of Goodwin's oscillators by periodic exogenous signals," in *Proc. of 54th IEEE Conf. on Decision and Control*, 2015, pp. 615–619.

[22] H. E. Samad, D. D. Vecchio, and M. Khammash, "Repressilators and promotilators: Loop dynamics in synthetic gene networks," in *Proc. of American Control Conference (ACC-2005)*, 2005, pp. 4405–4410.

[23] A. Churilov, A. Medvedev, and A. Shepelavyi, "Mathematical model of non-basal testosterone regulation in the male by pulse modulated feedback," *Automatica*, vol. 45, no. 1, pp. 78–85, 2009.

[24] P. Mattsson, A. Medvedev, and Z. Zhusubaliyev, "Pulse-modulated model of testosterone regulation subject to exogenous signals," in *Proceedings of the 55th IEEE Conference on Decision and Control*, Las Vegas, NE, December 2016.

[25] P. Mattsson and A. Medvedev, "Modeling of testosterone regulation by pulse-modulated feedback: an experimental data study," in *AIP Conference Proceedings*, vol. 1559, no. 1. AIP, 2013, pp. 333–342.

[26] ——, "Modeling of testosterone regulation by pulse-modulated feedback," in *Advances in Experimental Medicine and Biology*. Springer, 2015, vol. 823, pp. 23–40.

[27] V. S. Afraimovich and L. P. Shilnikov, "Invariant two-dimensional tori, their breakdown and stochasticity," *Amer. Math. Soc. Transl.*, vol. 149, pp. 201–211, 1991.